

UNIVERSIDAD SAN FRANCISCO DE QUITO USFQ

Colegio de Ciencias e Ingenierías

**OEDOMETRIC BEHAVIOR OF SOIL-DIATOM
MIXTURES BEFORE FRUSTULE CRACKING**

Marco Andrés Ribadeneira Flores

Ingeniería Civil

Trabajo de fin de carrera presentado como requisito

para la obtención del título de

Ingeniero Civil

Quito, 7 de diciembre de 2021

UNIVERSIDAD SAN FRANCISCO DE QUITO USFQ

Colegio de Ciencias e Ingenierías

HOJA DE CALIFICACIÓN DE TRABAJO DE FIN DE CARRERA

**Comportamiento edométrico de mezclas suelo-diatomea previo a la
ruptura de las frústulas**

Marco Andrés Ribadeneira Flores

Nombre del profesor, Título académico

Juan Pablo Villacreses, Msc. Ing. Vial

Quito, 7 de diciembre de 2021

DERECHOS DE AUTOR

Por medio del presente documento certifico que he leído todas las Políticas y Manuales de la Universidad San Francisco de Quito USFQ, incluyendo la Política de Propiedad Intelectual USFQ, y estoy de acuerdo con su contenido, por lo que los derechos de propiedad intelectual del presente trabajo quedan sujetos a lo dispuesto en esas Políticas.

Asimismo, autorizo a la USFQ para que realice la digitalización y publicación de este trabajo en el repositorio virtual, de conformidad a lo dispuesto en la Ley Orgánica de Educación Superior del Ecuador.

Nombres y apellidos: Marco Andrés Ribadeneira Flores

Código: 00200343

Cédula de identidad: 1750622290

Lugar y fecha: Quito, diciembre de 2021

ACLARACIÓN PARA PUBLICACIÓN

Nota: El presente trabajo, en su totalidad o cualquiera de sus partes, no debe ser considerado como una publicación, incluso a pesar de estar disponible sin restricciones a través de un repositorio institucional. Esta declaración se alinea con las prácticas y recomendaciones presentadas por el Committee on Publication Ethics COPE descritas por Barbour et al. (2017) Discussion document on best practice for issues around theses publishing, disponible en <http://bit.ly/COPETHeses>.

UNPUBLISHED DOCUMENT

Note: The following capstone project is available through Universidad San Francisco de Quito USFQ institutional repository. Nonetheless, this project – in whole or in part – should not be considered a publication. This statement follows the recommendations presented by the Committee on Publication Ethics COPE described by Barbour et al. (2017) Discussion document on best practice for issues around theses publishing available on <http://bit.ly/COPETHeses>.

RESUMEN

La presente investigación muestra los resultados de ensayos en laboratorio ocupados para caracterizar la compresibilidad en mezclas de suelo, las cuales fueron conformadas por suelo fino y la diatomea *Cyclotella Distinguenda*. La caracterización consistió en el análisis de los efectos del contenido de diatomeas en la consolidación de las mezclas antes de la ruptura-agrietamiento de las frústulas. Los ensayos implementados para definir las propiedades físicas de los especímenes ensayados incluyen al contenido de agua por masa, ensayo basado en el uso de la Cazuela de Casagrande para determinar el límite líquido, gravedad específica, y granulometría mediante el uso del hidrómetro. Por otra parte, el ensayo mecánico implementado para evaluar la compresibilidad de las muestras fue la consolidación unidimensional mediante el uso del edómetro. Como resultados, se evidenció una reducción del índice de compresión a mayor contenido de diatomea. A su vez, el coeficiente de consolidación incrementó al aumentar el contenido de diatomea, conduciendo a un proceso más rápido de disipación de la presión de poros. Con respecto a estos dos parámetros, dicho comportamiento está asociado a partículas de mayor diámetro aportadas en la mezcla por parte de las diatomeas. La presencia de estas partículas influye en el comportamiento de las muestras alterando su microestructura. Por lo tanto, las propiedades mencionadas de las mezclas fueron evaluadas con una condición de “no agrietamiento-ruptura” de las frústulas, presentando resultados de laboratorio con un comportamiento diferente al de reportes edométricos de la literatura actualmente registrada.

Palabras clave: Mezclas de diatomea, compresibilidad, ruptura-agrietamiento de partículas, contenido de diatomea

ABSTRACT

This paper presents the results of laboratory tests that characterized the compressibility of soil mixtures made of fine-grained soil and *Cyclotella Distinguenda* diatoms. The characterization analyzes the effects of diatom content on the consolidation of soil-diatom mixtures before the breakage of frustule particles. Laboratory tests implemented to define the physical properties of specimens include water content by mass, Casagrande test, specific gravity, and grain size distribution. Moreover, the mechanical test to evaluate compressibility was a one-dimensional oedometer test. The compressibility index of the samples decreased as the diatom content increased. Additionally, the coefficient of consolidation increases for a higher diatom content, leading to a faster process of pore water dissipation. Regarding the two parameters, this behavior is associated with a higher diameter of diatom particles when compared to clay soils. This bigger diameter influences the frictional characteristic of the soil samples, giving them sand-like properties. The tests evaluated the properties of soil-diatom mixtures with uncracked frustules showing a different behavior when compared to oedometer reports, and common soils.

Keywords: Diatom mixtures, compressibility, particle breakage, diatom content

TABLA DE CONTENIDOS

Introduction.....	11
Equations.....	12
Materials	13
Procedure	15
Results.....	16
Conclusiones	21
References.....	22
Anexo A: Time vs deformation experimental data for 0% diatom content.....	25
Anexo B: Time vs deformation experimental data for 20% diatom content	26
Anexo C: Time vs deformation experimental data for 40% diatom content	27
Anexo D: Time vs deformation experimental data for 60% diatom content.....	28

ÍNDICE DE TABLAS

Table #1. Properties of the tested samples.....	27
---	----

ÍNDICE DE FIGURAS

Figure #1. Scanning electron microscopy (SEM) of <i>Cyclotella Distinguenda</i> diatoms.....	27
Figure #2. Fine-grained soil particle size distribution	15
Figure #3. Diatom particle size distribution	15
Figure #4. Liquid limits of the tested samples	18
Figure #5. Consolidation curves of tested samples.....	18
Figure #6. Compression index of the tested samples.....	19
Figure #7. Swell index of tested samples.....	19
Figure #8. Relationship between C_c and W_L	19
Figure #9. Coefficient of consolidation of tested samples.....	20

Disclaimer

This project consists of a short academic paper written by me. It contains the procedure and results of an investigation that was conducted during the last semester of Civil Engineering. It was intended to be presented in a scientific magazine until the last days of December, waiting for an acceptance of submission to be published.

The presented document is subject to the clarification for publication of the San Francisco University of Quito. For that reason, it is requested that this paper could be used without restrictions for future publication. Also, the presented information is considered as an original work classified as unpublished work. This justifies the possibility of submitting this manuscript to a journal or magazine for publication, even if the work is available via the university repository.

OEDOMETRIC BEHAVIOR OF SOIL-DIATOM MIXTURES BEFORE FRUSTULE CRACKING

Laura Ibagón^{1,2}, Bernardo Caicedo¹, Marco Ribadeneira², Juan P. Villacreses^{1,2},

Fabricio Yepez²,

¹Universidad de los Andes

Cr. 1 #18a, Bogotá, Colombia

jp.villacreses@uniandes.edu.co; fyepez@usfq.edu.ec

²Universidad San Francisco de Quito

Pampite, Quito, Ecuador.

Abstract – This paper presents the results of laboratory tests that characterized the compressibility of soil mixtures made of fine-grained soil and *Cyclotella Distinguenda* diatoms. The characterization analyzes the effects of diatom content on the consolidation of soil-diatom mixtures before the breakage of frustule particles. Laboratory tests implemented to define the physical properties of specimens include water content by mass, Casagrande test, specific gravity, and grain size distribution. Moreover, the mechanical test to evaluate compressibility was a one-dimensional oedometer test. The compressibility index of the samples decreased as the diatom content increased. Additionally, the coefficient of consolidation increases for a higher diatom content, leading to a faster process of pore water dissipation. Regarding those two parameters, this behavior is associated with a higher diameter of diatom particles when compared to clay soils. This bigger diameter influences the frictional characteristic of the soil samples, giving them sand-like properties. The tests evaluated the properties of soil-diatom mixtures with uncracked frustules showing a different behavior when compared to oedometer reports, and common soils.

Keywords: Diatom mixtures, compressibility, particle breakage, diatom content

1. INTRODUCTION

Geotechnical characteristics of soft soils like diatomaceous soils are important to analyze the performance of engineering constructions. Structures placed over these deposits may have considerable settlements due to the low bearing capacity of diatomaceous soils (Caicedo, Mendoza, López, & Lizcano, 2018). These diatomaceous soils are natural lacustrine and marine deposits that can be found in areas with high concentrations of phytoplankton and volcanic activity that promotes silica production. Countries that satisfy these requirements are typically the ones near the Pacific fire belt, such as Colombia, Chile, Mexico, among others (Caicedo et al., 2019).

Diatomaceous soil deposits are conformed by fossilized frustules and fine-grained material. The frustules are the external siliceous shell that protects the unicellular algae against predators (Hamm, y otros, 2003). Diatom frustules are sedimented once their organic matter has decomposed, remaining in the soil throughout geological ages (Caicedo, Zuluaga, & Slebi, 2019). These microfossils generally have symmetrical shapes with a similar size to silt soil particles. However, the shape of the particles contains voids that cause high Atterberg limits when trying to characterize the material (Perisic, Ovalle, & Barrios, 2019). The content of diatoms, loading history, and stress level, modify the mechanical response of soil-diatom mixtures, changing their compressibility, shear strength, void ratio, and water content (Sonyok & Bandini, 2019).

Diatomaceous soil has counterintuitive properties based on its mechanical behavior. For instance, diatoms have high water carrying capacity due to the shape of the frustule, but when the samples are classified, their behavior is associated with non-plastic materials. Also, it is necessary to consider the content of fossilized frustules in the mixture, since diatomaceous soils behave as plastic materials for diatomite content less than 50% (Caicedo et al., 2019).

Important laboratory research on diatomaceous soils has been developed in the past few years. However, there still exist variables to evaluate, such as the behavior of soil-diatom mixtures before frustule cracking.

Laboratory tests were conducted in mixtures made of fine-grained soil with a varying percentage of diatom *Cyclotella Distinguenda* to characterize their compressibility, geotechnical properties, and index properties. The compressibility results of samples using the oedometer test are discussed in this investigation when the diatom frustules have not reached the yielding stress.

2. EQUATIONS

Test procedures and equations were based on ASTM specifications to calculate the physical and index properties of samples. The specific gravity by water pycnometer, the water content, and the liquid limit were computed according to ASTM D854-02 (Method A) (D854-02, 2002), ASTM D2216-19 (Method A) (D2216-19, 2019), and ASTM D4318-00 (Method A) (D4318-00, 2000), respectively. The oedometer test procedure was applied according to ASTM D2435-03 (D2435-03, 2003), and the calculations were based on the standard method “Taylor square root of time”. This method estimates the time corresponding to the 90% primary compression point to calculate the coefficient of consolidation (C_v). (Shukla et al., 2009).

The oedometer test was used to compute the compressibility parameters (i.e., C_c and C_v). Time (t) - deformation (s) curves were obtained during the test for each step of loading according to the diatom content (DC) on the mixture. Changes in the void ratio (Δe_1), and the final void ratio (e_1), were calculated using the initial dimensions of each sample (height of soils - H_s , the initial height of voids – H_v , and initial void ratio – e_0). The mentioned data was processed using calculation tables to plot the consolidation curve (σ' vs e) for each mixture.

Finally, the compression index (C_c) and swell index (C_s) were obtained graphically analyzing the consolidation curves.

To define the time corresponding to a 90% primary consolidation (t_{90}) the graphical method “square root of time” was implemented. After analyzing the t_{90} for each load increment on the corresponding diatom content, C_v was calculated with equation (1) (Shukla et al., 2009). The use of this equation requires a time factor (T_v) that considers the velocity of flow in the z-direction (v_z) for a one-dimensional consolidation test. This factor, presented by Shukla et al, assumes a constant initial excess pore water pressure throughout the depth of small samples. The value of T_v is taken as 0.848 for the 90% average degree of primary consolidation (Shukla et al., 2009).

$$C_v = \frac{T_v * (H_{dr})^2}{t_{90}} \quad (1)$$

Where:

T_v is the time factor.

H_{dr} is the average longest drainage path during consolidation.

t_{90} is the time corresponding to the 90% primary consolidation.

3. MATERIALS

Cyclotella Distinguenda diatoms (D) and commercial fine-grained soil (S) were used to create the different samples. This kind of diatom is disc-shaped with central symmetry. The valve of the diatom frustule presents a circular center tangentially undulate with an external stria contour. Furthermore, the smooth central area conforms 30% to 50% of the valve face

(Hustedt, 1927). Additionally, the SEM image of Figure 1 shows the shape and initial condition of the tested diatom.

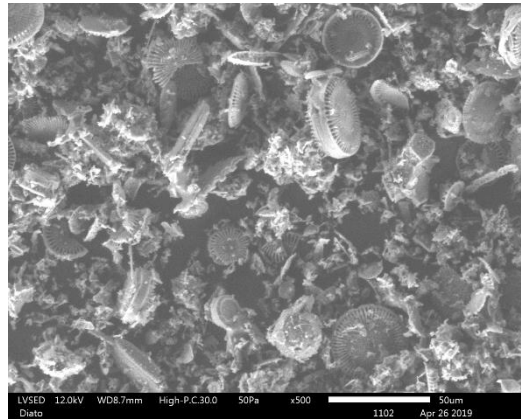


Fig. #1: Scanning electron microscopy (SEM) of *Cyclotella Distinguenda* diatoms

Physical properties for five different soil-diatom mixtures are summarized in Table 1. The specimens were prepared with the following diatom contents: 0% 20%, 40%, and 60%. Median particle size (D_{50}) and the water content (W%) were reported in Table 1 just for pure materials, represented as 0% (S) and 100% (D). Also, there are no values of liquid limit (W_L), C_c , and C_s for 100% of DC due to the limitations present in ASTM tests.

Table #1: Properties of the tested samples

Mixture	Fine-grained Soil Content (%)	Diatomite Content (%)	Gs	D_{50} (μm)	Plastic Limit (%)	Liquid Limit (%)	C_s	C_c
1	100	0	2,65	1,2	23	37	0,007	0,28
2	80	20	2,58	-	32	39	0,011	0,20
3	60	40	2,51	-	Not Achieved	46	0,026	0,11
4	40	60	2,44	-	Not Achieved	75	0,026	0,08
5	0	100	2,32	8,5	Not Achieved	-	-	-

The plastic limit test according to the ASTM D4318-00 specification was applied on each specimen. Values for samples 2, 3, and 4 are not reported because thixotropic properties

compromised the results. For that reason, the liquid limits (W_L) shown in Table 1 are used as indicators of the water carrying capacity.

Particle size distribution for S and D was constructed using the hydrometer test according to ASTM D422-63 (D422-63, 2002). Figure 2 shows the particle size distribution curve for S and D. Analyzing the D_{50} , W_P , and W_L of S, the particle size of the specimen can be considered as a passing material for sieve N° 200. Therefore, according to ASTM D2487-17, this soil can be classified as low plasticity clay (CL) (D2487-17, 2017).

Figure 3 shows the particle size distribution curve for the *Cyclotella Distinguenda* diatom (D). The D_{50} and W_L were used to characterize the diatoms using $W_P = 0$. Consequently, the three S-D mixtures were classified as sandy silt (ML).

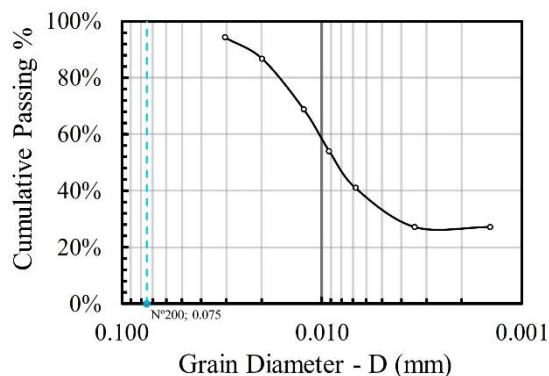


Fig. #2: Fine-grained soil particle size distribution

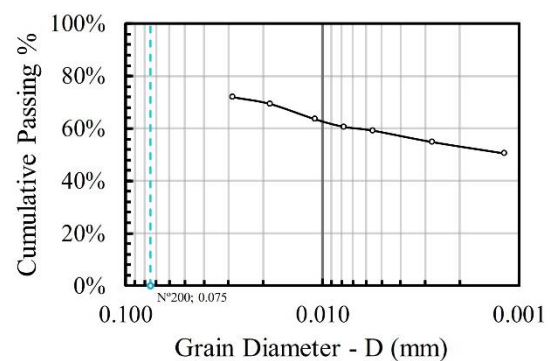


Fig. #3: Diatom particle size distribution

distribution

4. PROCEDURE

The laboratory tests implemented in this research consisted of physical and mechanical tests. Physical tests included water content by mass, Casagrande test (W_L test), plastic limit test, specific gravity by water pycnometer, and grain size distribution by hydrometer test. The

mechanical test to evaluate compressibility was a one-dimensional oedometer test. Procedures for these tests were based on ASTM specifications.

The characterization of fine-grained soil and diatom specimens with physical tests is summarized in Table 1, Figure 2, and Figure 3. Four remolded samples were used for the one-dimensional oedometer test following diatom contents of 0%, 20%, 40%, and 60% by dry mass. These samples were prepared with a water content of 1.5 times their Liquid Limit. This W_L was used to erase the geological pressure history of the samples (Chamorro Cardona et al., 2004). In addition, the samples were pre-consolidated to 0.45 kPa to stand the weight of the mechanism.

The consolidation process was developed in a conventional oedometer under saturated conditions. Samples were prepared with two porous stone discs at the top and bottom of the consolidation mold. The load increment ratio used for loading and unloading cycles presented the following stress steps: 4, 8, 15.5, 31, and 62 kPa. These stresses are selected because they are sufficiently lower compared to the yielding stress of diatom particles (Sonyok & Bandini, 2019). Loading and unloading cycles were completed in approximately 2 days. The end of primary consolidation was monitored with the Taylor Method – square root of time, defining enough values during tests to compute the t_{90} . As a result, the tested samples were 63.4 mm in diameter, 13.53 mm as a constant initial height, and a final height that varies according to the sample.

5. RESULTS

Figure 4 shows the liquid limit of the mixtures for different DC. The curve shows an increment in W_L as the diatom content increases. Consequently, the water storage capacity of the sample rises due to the intraparticle porosities within frustules. This property explains the

high W_L and low dry density on samples with higher diatom content (Ovalle & Arenaldi-Perisic, 2021).

Despite the W_L increases at high DC, the W_P could not be determined with the ASTM D4118-00 specifications. Regarding the mentioned ASTM, its application evidenced the thixotropic properties on the remolded samples. This behavior justifies the indeterminacy of W_P , leading to presume that the mixture could behave as non-plastic (Ovalle & Arenaldi-Perisic, 2021).

The oedometer test results were used to plot the samples' variation of height in time, distinguishing load increments and DCs. These results were analyzed to compute the consolidation curve presented in Figure 5. In addition, the geologic pressure history of the specimens was erased (Chamorro Cardona et al., 2004), allowing the obtainment of the virgin compression curve for the samples with lower vertical stress steps.

Figure 5 shows an increment of e_o at high DC due to the intraparticle porosity of frustules. The following values of e_o were registered for 0%, 20%, 40% and 60% DC: 0.82, 0.90, 1.71 and 2.37 respectively. Moreover, the distance between the curves of loading and unloading cycles shows a reduction of compressibility at higher DC. Oedometer results of researchers such as Caicedo et. al (Caicedo et al., 2019) and Sonyok & Bandini (Sonyok & Bandini, 2019), used pre-consolidation stresses between 30 and 60 kPa, and a maximum stress step between 800 and 1000 kPa. Those testing values resulted in higher compressibility at higher diatom contents. The mentioned test reports differ from the values of this paper. Therefore, the reduction of compressibility at higher DC is reduced due to frustules not being crushed.

Materials with 65% of diatom microfossils presented high frustule crushing at large stresses (up to 1600 kPa) (Sonyok & Bandini, 2019). Besides, the breakage of microfossils at higher stress levels depends on the frustules' composition, geometry, size, and orientation (Sonyok & Bandini, 2019). The applied short-term one-dimensional oedometer tests reached a maximum

stress step of 62 kPa. For that reason, the tested specimens showed an initial gradual compression that did not generate a disturbance of the soil microstructure by cracking. However, the data presented some volumetric deformations due to short compression of the interparticle pore voids (Sonyok & Bandini, 2019).

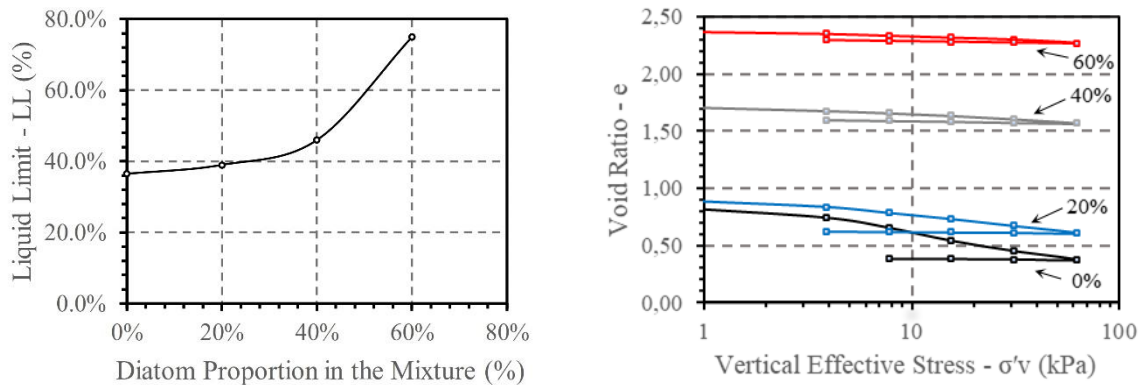


Fig. #4: Liquid limits of the tested samples Fig. #5: Consolidation curves of tested samples

From Figure 5 the C_c and C_s parameters were registered on Figures 6 and 7 in terms of C_c – diatom content (%) and C_s – diatom content (%) respectively. Figure 6 shows the compression index for the different diatom contents on samples. The following values of C_c were registered for 0%, 20%, 40% and 60% DC: 0.28, 0.20, 0.11, and 0.08 respectively. Those values show a reduction of C_c at higher DC due to frustules crushing as formerly explained. The non-disturbance of the soil microstructure meant lower compressibility.

Figure 7 shows the swell index with the following values for 0%, 20%, 40% and 60% DC: 0.007, 0.011, 0.026, and 0.026 respectively. The increment of C_s at higher DC justifies the high strength against compression due to the uncracked frustules. Also, the compressive strength of frustules presents elastic deformations under high compressive stresses, until they cracked under a brittle failure. Hence, the increase of swell index is justified by the uncracked frustules and the recovering of elastic compression in some diatomite particles during the unloading cycle (Sonyok & Bandini, 2019).

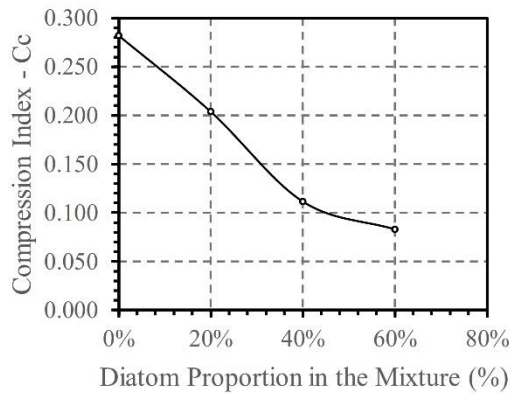


Fig. 6: Compression index of the tested samples

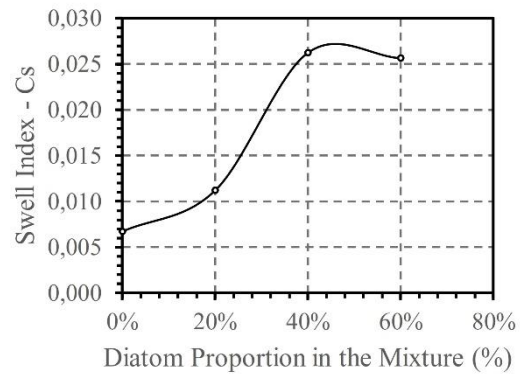
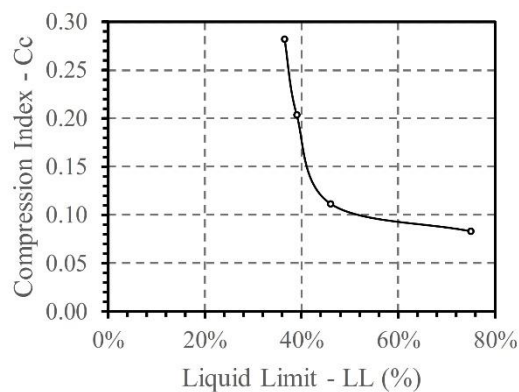


Fig. 7: Swell index of tested samples

Figure 8 shows the relationship between the liquid limit and the compression index. The effects of higher DC are seen in increments of W_L and decrements of C_c , as shown in Figures 4 and 6 respectively. As a result, C_c decreases at higher W_L in the tested S-D mixtures. These results are based on the uncracked state of the diatom frustules. The increase of diatom content induces a higher compressive strength, despite the increase of void space. Otherwise, if the stress surpasses the elastic compression of the frustules, the behavior of the mixture could tend to an increment of C_c at higher W_L , due to the release of trapped water after diatom crushing (Caicedo et al., 2019).

Fig 8: Relationship between C_c and W_L

The coefficient of consolidation (C_v) was computed with the graphic method of the square root of time suggested by Taylor. Figure 9 shows an increment of C_v at higher DC and higher vertical stresses. Comparing the C_v variation between DC of 0% to 20%, 20% to 40%, and 40% to 60%, the highest value corresponding to that of 20% to 40%. This is also seen in Figure 5, with a higher increment of e_o associated to the sample with 40% DC. These data demonstrate that the tested fine-grained soil didn't get higher fabric modifications at diatom contents up to 20%.

On the other hand, the increase of C_v at higher diatom content is supported by a faster pore pressure dissipation due to a higher porosity of the mixture. The high content of voids in diatom frustules influences the water carrying capacity of the mixture. This results in more drainage of the S-D samples under higher vertical stresses due to larger intraparticle gaps. Hence, the porosity of the mixtures made of intraparticle and interparticle voids expels water faster than the fine soil specimen by itself. In addition, this behavior makes the consolidation process faster at higher DC, considering that the behavior of uncracked frustules results in less volumetric deformations on the samples.

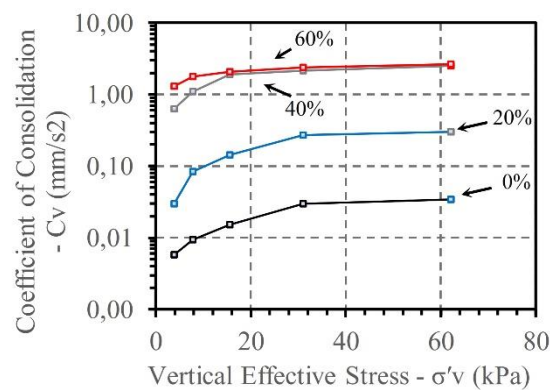


Fig 9: Coefficient of consolidation of tested samples

6. CONCLUSIONS

This paper presents the results of physical and mechanical laboratory tests to characterize the compressibility of soil mixtures made of fine-grained soil and a varying percentage of *Cyclotella Distinguenda* diatom. Four remolded samples were used for the one-dimensional oedometer test following diatom contents of 0%, 20%, 40%, and 60% by dry mass. Those samples were tested with stress steps under the yielding stress of the soil-diatom mixtures. As a result, the following characteristics were defined for the mixtures tested before the breakage of frustule particles:

- The increase of DC in the samples modified its microstructure, getting larger intraparticle porosities due to the voids within diatom frustules. Moreover, diatoms had a particle size bigger than the fine-grained soil that incremented the interparticle porosities of the mixture. Those characteristics justify the increased W_L , e_o , and the low dry specific gravity of the samples at higher DC.
- The maximum stress step applied in oedometer tests was lower than the one reported on the used references of Caicedo et. al (Caicedo et al., 2019) and Sonyok & Bandini (Sonyok & Bandini, 2019). Consequently, the yielding stress of fractures was not reached. The results suggest that C_c reduces as DC increases, which opposes the mentioned oedometer reports.
- The compressibility index of S-D samples had a reduction at higher DC due to an improvement in their compressive strength. That improvement depends on the uncracked condition of diatom frustules. An increment of diatom content results in lower compressibility due to the higher resistance of hard siliceous frustules.
- The swell index of the tested samples had an increment at higher DC due to the recovering of elastic compression in some diatomite particles. Hence, some

volumetric deformations on the unloading cycle were explained by short compressions of the interparticle and intraparticle porosities of the mixtures.

- The coefficient of consolidation had an increment at higher DC due to faster pore pressure dissipation. This could be explained by the diatom porosities, which had a bigger size than the ones of the fine-grained soil. That microstructure modification on samples results in more drainage that accelerates the consolidation process.

The obtained results from this paper show a different behavior of the soil-diatom mixtures compared to other oedometer tests. Otherwise, the showed characteristics become an important contribution to oedometric tests when the diatom frustules have not reached the yielding stress. For instance, this behavior can be a reference to future implemented tests that could present properties similar to the ones presented in this paper. In addition, this information promotes the investigation regarding the yielding stress of this kind of soil, also considering other variables such as the geometry of frustules, or the effect of creep for stresses lower than the yielding one.

7. REFERENCES

- Caicedo, B., Mendoza, C., Lizcano, A., & Lopez-Caballero, F. (2019). Some contributions to mechanical behaviors of lacustrine deposit in Bogotá, Colombia. *Journal of Rock Mechanics and Geotechnical Engineering*, *11*, 837–849.
- Caicedo, B., Mendoza, C., López, F., & Lizcano, A. (2018). Behavior of diatomaceous soil in lacustrine deposits of Bogotá, Colombia. *Journal of Rock Mechanics and Geotechnical Engineering*, *10*, 367–379.
- Caicedo, B., Zuluaga, D., & Slebi, C. (2019). Effects of micro-features of fossil diatom on the macroscopic behaviour of soils. *Géotechnique Letters*, *9*, 322–327.

- Chamorro Cardona, J. C., & others. (2004). *Modelación en centrífuga de túneles poco profundos en arcillas de la Sabana de Bogotá*. Master's thesis, Uniandes.
- D2216-19, A. S. (2019). Standard Test Methods for Laboratory Determination of Water (Moisture) Content of Soil and Rock by Mass. *ASTM International*, 04.08, 7.
- D2435-03, A. S. (2003). Standard Test Method for One-Dimensional Consolidation Properties of Soils. *ASTM International*, 04.08, 10.
- D2487-17, A. S. (2017). Standard Practice for Classification of Soils for Engineering Purposes (Unified Soil Classification System). *ASTM International*, 04.08, 10.
- D422-63, A. S. (2002). Standard Test Method for Particle-Size Analysis of Soils. *ASTM International*, 04.08, 8.
- D4318-00, A. S. (2000). Standard Test Methods for Liquid Limit, Plastic Limit, and Plasticity Index of Soils. *ASTM International*, 04.08, 14.
- D854-02, A. S. (2002). Standard Test Methods for Specific Gravity of Soil Solids by Water Pycnometer. *ASTM International*, 04.08, 7.
- Hamm, C. E., Merkel, R., Springer, O., Jurkojc, P., Maier, C., Prechtel, K., & Smetacek, V. (2003). Architecture and material properties of diatom shells provide effective mechanical protection. *Nature*, 421, 841–843.
- Hustedt, F. (1927). Die Diatomeen der interstadialen Seekreide. *H. Gams, Die Geschichte der Lunzer Seen, Moore und Wälder. Internationale Revue der gesamten Hydrobiologie*, 18, 305–387.
- Ovalle, C., & Arenaldi-Perisic, G. (2021). Mechanical behaviour of undisturbed diatomaceous soil. *Marine Georesources & Geotechnology*, 39, 623–630.
- Perisic, G. A., Ovalle, C., & Barrios, A. (2019). Compressibility and creep of a diatomaceous soil. *Engineering Geology*, 258, 105145.
- Shukla, S., Sivakugan, N., & Das, B. (2009). Methods for determination of the coefficient of consolidation and field observations of time rate of settlement—an overview. *International Journal of Geotechnical Engineering*, 3, 89–108.

Sonyok, D. R., & Bandini, P. (2019). Oedometric Behavior of Diatomite–Kaolin Mixtures. *Journal of Geotechnical and Geoenvironmental Engineering*, 145, 06019005.

ANEXO A: TIME VS DEFORMATION EXPERIMENTAL DATA FOR 0% DIATOM CONTENT

Loading Cycle - 4 kPa		
Time (t) [min]	Square root of time [min]	Deformation (s) [mm]
0.0	0.00	7.16
0.1	0.32	7.12
0.2	0.45	7.11
0.4	0.63	7.10
0.6	0.77	7.09
1.0	1.00	7.09
2.0	1.41	7.08
4.0	2.00	7.05
6.0	2.45	7.03
10.0	3.16	6.99
20.0	4.47	6.92
40.0	6.32	6.79
60.0	7.75	6.71
100.0	10.00	6.63
165.0	12.85	6.59
200.0	14.14	6.58

Loading Cycle - 8 kPa		
Time (t) [min]	Square root of time [min]	Deformation (s) [mm]
0.0	0.00	6.40
0.1	0.32	6.38
0.2	0.45	6.37
0.4	0.63	6.36
0.6	0.77	6.35
1.0	1.00	6.33
2.0	1.41	6.29
4.0	2.00	6.23
6.0	2.45	6.19
10.0	3.16	6.12
20.0	4.47	6.01
40.0	6.32	5.89
60.0	7.75	5.83
101.0	10.05	5.78
165.0	12.85	5.75
200.0	14.14	5.74

Loading Cycle - 15.5 kPa		
Time (t) [min]	Square root of time [min]	Deformation (s) [mm]
0.0	0.00	6.90
0.1	0.32	6.86
0.2	0.45	6.85
0.4	0.63	6.83
0.6	0.77	6.81
1.0	1.00	6.78
2.0	1.41	6.72
4.0	2.00	6.64
6.0	2.45	6.57
10.0	3.16	6.47
20.0	4.47	6.29
41.0	6.40	6.12
60.0	7.75	6.07
100.0	10.00	6.04

Loading Cycle - 31 kPa		
Time (t) [min]	Square root of time [min]	Deformation (s) [mm]
0.0	0.00	9.95
0.1	0.32	9.92
0.2	0.45	9.90
0.4	0.63	9.88
0.6	0.77	9.86
1.0	1.00	9.83
2.0	1.41	9.77
4.0	2.00	9.68
6.0	2.45	9.62
10.0	3.16	9.52
23.0	4.80	9.37
40.0	6.32	9.31
60.0	7.75	9.29
100.0	10.00	9.28

Loading Cycle - 62 kPa		
Time (t) [min]	Square root of time [min]	Deformation (s) [mm]
0.0	0.00	9.28
0.1	0.32	9.20
0.2	0.45	9.18
0.4	0.63	9.16
0.6	0.77	9.15
1.0	1.00	9.12
2.0	1.41	9.07
4.0	2.00	8.99
6.0	2.45	8.94
10.0	3.16	8.86
20.0	4.47	8.77
40.0	6.32	8.72
60.0	7.75	8.71
100.0	10.00	8.70

Unloading Cycle - 31 kPa		
Time (t) [min]	Square root of time [min]	Deformation (s) [mm]
0.0	0.00	8.76
0.1	0.32	8.76
0.2	0.45	8.76
0.4	0.63	8.76
0.6	0.77	8.76
1.0	1.00	8.76
2.0	1.41	8.77
4.0	2.00	8.77
6.0	2.45	8.77
10.0	3.16	8.78
20.0	4.47	8.78
40.0	6.32	8.79

Unloading Cycle - 15.5 kPa		
Time (t) [min]	Square root of time [min]	Deformation (s) [mm]
0.0	0.00	8.80
0.1	0.32	8.80
0.2	0.45	8.80
0.4	0.63	8.80
0.6	0.77	8.80
1.0	1.00	8.80
2.0	1.41	8.80
4.0	2.00	8.80
6.0	2.45	8.81
10.0	3.16	8.81
20.0	4.47	8.81
40.0	6.32	8.82

Unloading Cycle - 8 kPa		
Time (t) [min]	Square root of time [min]	Deformation (s) [mm]
0.0	0.00	8.85
0.1	0.32	8.85
0.2	0.45	8.85
0.4	0.63	8.85
0.6	0.77	8.85
1.0	1.00	8.85
2.0	1.41	8.86
4.0	2.00	8.86
6.0	2.45	8.86
10.0	3.16	8.86
20.0	4.47	8.86

ANEXO B: TIME VS DEFORMATION EXPERIMENTAL DATA FOR 20% DIATOM CONTENT

Loading Cycle - 4 kPa		
Time (t) [min]	Square root of time [min]	Deformation (s) [mm]
0.0	0.00	15.70
0.1	0.32	15.69
0.2	0.45	15.69
0.4	0.63	15.68
0.6	0.77	15.66
1.0	1.00	15.65
2.0	1.41	15.62
4.0	2.00	15.58
6.0	2.45	15.54
10.0	3.16	15.46
20.0	4.47	15.37
40.0	6.32	15.35
60.0	7.75	15.34
100.0	10.00	15.34

Loading Cycle - 8 kPa		
Time (t) [min]	Square root of time [min]	Deformation (s) [mm]
0.0	0.00	15.23
0.1	0.32	15.20
0.2	0.45	15.18
0.4	0.63	15.16
0.6	0.77	15.14
1.0	1.00	15.11
2.0	1.41	15.05
4.0	2.00	14.99
6.0	2.45	14.96
10.0	3.16	14.92
20.0	4.47	14.89
40.0	6.32	14.87
60.0	7.75	14.87
100.0	10.00	14.86

Loading Cycle - 15.5 kPa		
Time (t) [min]	Square root of time [min]	Deformation (s) [mm]
0.0	0.00	14.74
0.1	0.32	14.71
0.2	0.45	14.69
0.4	0.63	14.66
0.6	0.77	14.63
1.0	1.00	14.59
2.0	1.41	14.52
4.0	2.00	14.46
6.0	2.45	14.43
10.0	3.16	14.40
20.0	4.47	14.38
40.0	6.32	14.37
60.0	7.75	14.36

Loading Cycle - 31 kPa		
Time (t) [min]	Square root of time [min]	Deformation (s) [mm]
0.0	0.00	14.25
0.1	0.32	14.19
0.2	0.45	14.16
0.4	0.63	14.12
0.6	0.77	14.09
1.0	1.00	14.04
2.0	1.41	13.98
4.0	2.00	13.91
6.0	2.45	13.88
10.0	3.16	13.86
20.0	4.47	13.84
40.0	6.32	13.83
60.0	7.75	13.82

Loading Cycle - 62 kPa		
Time (t) [min]	Square root of time [min]	Deformation (s) [mm]
0.0	0.00	13.69
0.1	0.32	13.64
0.2	0.45	13.59
0.4	0.63	13.54
0.6	0.77	13.50
1.0	1.00	13.45
2.0	1.41	13.37
4.0	2.00	13.32
6.0	2.45	13.30
10.0	3.16	13.28
20.0	4.47	13.26
40.0	6.32	13.25
60.0	7.75	13.24

Unloading Cycle - 31 kPa		
Time (t) [min]	Square root of time [min]	Deformation (s) [mm]
0.0	0.00	13.23
0.1	0.32	13.24
0.2	0.45	13.24
0.4	0.63	13.24
0.6	0.77	13.25
1.0	1.00	13.25
2.0	1.41	13.25
4.0	2.00	13.25
6.0	2.45	13.25
10.0	3.16	13.25
20.0	4.47	13.25
40.0	6.32	13.25

Unloading Cycle - 15.5kPa		
Time (t) [min]	Square root of time [min]	Deformation (s) [mm]
0.0	0.00	13.26
0.1	0.32	13.27
0.2	0.45	13.27
0.4	0.63	13.27
0.6	0.77	13.27
1.0	1.00	13.28
2.0	1.41	13.28
4.0	2.00	13.28
6.0	2.45	13.28
10.0	3.16	13.28
20.0	4.47	13.28
40.0	6.32	13.28
60.0	7.75	13.28

Unloading Cycle - 8 kPa		
Time (t) [min]	Square root of time [min]	Deformation (s) [mm]
0.0	0.00	13.29
0.1	0.32	13.30
0.2	0.45	13.31
0.4	0.63	13.31
0.6	0.77	13.31
1.0	1.00	13.31
2.0	1.41	13.31
4.0	2.00	13.31
6.0	2.45	13.32
10.0	3.16	13.32
20.0	4.47	13.32
40.0	6.32	13.32

Unloading Cycle - 4 kPa		
Time (t) [min]	Square root of time [min]	Deformation (s) [mm]
0.0	0.00	13.33
0.1	0.32	13.34
0.2	0.45	13.34
0.4	0.63	13.34
0.6	0.77	13.34
1.0	1.00	13.35
2.0	1.41	13.35
4.0	2.00	13.35
6.0	2.45	13.35
10.0	3.16	13.35
20.0	4.47	13.35
40.0	6.32	13.35

ANEXO C: TIME VS DEFORMATION EXPERIMENTAL DATA FOR 40% DIATOM CONTENT

Loading Cycle - 4 kPa		
Time (t) [min]	Square root of time [min]	Deformation (s) [mm]
0.0	0.00	14.15
0.1	0.32	14.09
0.2	0.45	14.07
0.4	0.63	14.05
0.6	0.77	14.04
1.0	1.00	14.02
2.0	1.41	14.01
4.0	2.00	14.00
6.0	2.45	14.00
10.0	3.16	13.99
20.0	4.47	13.99
40.0	6.32	13.99

Loading Cycle - 8 kPa		
Time (t) [min]	Square root of time [min]	Deformation (s) [mm]
0.0	0.00	13.95
0.1	0.32	13.91
0.2	0.45	13.90
0.4	0.63	13.89
0.6	0.77	13.89
1.0	1.00	13.88
2.0	1.41	13.88
4.0	2.00	13.87
6.0	2.45	13.87
10.0	3.16	13.86
20.0	4.47	13.86
40.0	6.32	13.85

Loading Cycle - 15.5 kPa		
Time (t) [min]	Square root of time [min]	Deformation (s) [mm]
0.0	0.00	13.74
0.1	0.32	13.71
0.2	0.45	13.69
0.4	0.63	13.68
0.6	0.77	13.68
1.0	1.00	13.67
2.0	1.41	13.66
4.0	2.00	13.65
6.0	2.45	13.65
10.0	3.16	13.64
20.0	4.47	13.63
40.0	6.32	13.63

Loading Cycle - 31 kPa		
Time (t) [min]	Square root of time [min]	Deformation (s) [mm]
0.0	0.00	13.49
0.1	0.32	13.44
0.2	0.45	13.43
0.4	0.63	13.42
0.6	0.77	13.41
1.0	1.00	13.40
2.0	1.41	13.39
4.0	2.00	13.38
6.0	2.45	13.38
10.0	3.16	13.37
20.0	4.47	13.35
40.0	6.32	13.34

Loading Cycle - 62 kPa		
Time (t) [min]	Square root of time [min]	Deformation (s) [mm]
0.0	0.00	13.12
0.1	0.32	13.07
0.2	0.45	13.06
0.4	0.63	13.04
0.6	0.77	13.04
1.0	1.00	13.02
2.0	1.41	13.01
4.0	2.00	12.99
6.0	2.45	12.98
10.0	3.16	12.97
20.0	4.47	12.95
40.0	6.32	12.94

Unloading Cycle - 31 kPa		
Time (t) [min]	Square root of time [min]	Deformation (s) [mm]
0.0	0.00	12.94
0.1	0.32	12.96
0.2	0.45	12.96
0.4	0.63	12.96
0.6	0.77	12.97
1.0	1.00	12.97
2.0	1.41	12.97
4.0	2.00	12.97
6.0	2.45	12.97
10.0	3.16	12.97
20.0	4.47	12.97

Unloading Cycle - 15.5 kPa		
Time (t) [min]	Square root of time [min]	Deformation (s) [mm]
0.0	0.00	12.97
0.1	0.32	13.01
0.2	0.45	13.01
0.4	0.63	13.01
0.6	0.77	13.01
1.0	1.00	13.02
2.0	1.41	13.02
4.0	2.00	13.02
6.0	2.45	13.02
10.0	3.16	13.02
20.0	4.47	13.02

Unloading Cycle - 8 kPa		
Time (t) [min]	Square root of time [min]	Deformation (s) [mm]
0.0	0.00	13.03
0.1	0.32	13.06
0.2	0.45	13.06
0.4	0.63	13.06
0.6	0.77	13.06
1.0	1.00	13.06
2.0	1.41	13.06
4.0	2.00	13.06
6.0	2.45	13.06
10.0	3.16	13.07
20.0	4.47	13.07

Unloading Cycle - 4 kPa		
Time (t) [min]	Square root of time [min]	Deformation (s) [mm]
0.0	0.00	13.08
0.1	0.32	13.09
0.2	0.45	13.10
0.4	0.63	13.10
0.6	0.77	13.10
1.0	1.00	13.11
2.0	1.41	13.11
4.0	2.00	13.11
6.0	2.45	13.11
10.0	3.16	13.11
20.0	4.47	13.11

ANEXO D: TIME VS DEFORMATION EXPERIMENTAL DATA FOR 60% DIATOM CONTENT

Loading Cycle - 4kPa		
Time (t) [min]	Square root of time [min]	Deformation (s) [mm]
0.0	0.00	18.27
0.1	0.32	18.25
0.2	0.45	18.24
0.4	0.63	18.22
0.6	0.77	18.22
1.0	1.00	18.22
2.0	1.41	18.22
4.0	2.00	18.21
6.0	2.45	18.21
10.0	3.16	18.21
20.0	4.47	18.20
40.0	6.32	18.20

Loading Cycle - 8kPa		
Time (t) [min]	Square root of time [min]	Deformation (s) [mm]
0.0	0.00	18.12
0.1	0.32	18.10
0.2	0.45	18.10
0.4	0.63	18.09
0.6	0.77	18.09
1.0	1.00	18.08
2.0	1.41	18.08
4.0	2.00	18.07
6.0	2.45	18.07
10.0	3.16	18.07
20.0	4.47	18.06
40.0	6.32	18.06

Loading Cycle - 15.5 kPa		
Time (t) [min]	Square root of time [min]	Deformation (s) [mm]
0.0	0.00	17.95
0.1	0.32	17.94
0.2	0.45	17.93
0.4	0.63	17.93
0.6	0.77	17.92
1.0	1.00	17.92
2.0	1.41	17.91
4.0	2.00	17.91
6.0	2.45	17.90
10.0	3.16	17.90
20.0	4.47	17.89
40.0	6.32	17.88

Loading Cycle - 31 kPa		
Time (t) [min]	Square root of time [min]	Deformation (s) [mm]
0.0	0.00	17.75
0.1	0.32	17.73
0.2	0.45	17.72
0.4	0.63	17.72
0.6	0.77	17.71
1.0	1.00	17.70
2.0	1.41	17.70
4.0	2.00	17.69
6.0	2.45	17.69
10.0	3.16	17.68
20.0	4.47	17.68

Loading Cycle - 62 kPa		
Time (t) [min]	Square root of time [min]	Deformation (s) [mm]
0.0	0.00	17.45
0.1	0.32	17.42
0.2	0.45	17.41
0.4	0.63	17.40
0.6	0.77	17.39
1.0	1.00	17.38
2.0	1.41	17.37
4.0	2.00	17.35
6.0	2.45	17.34
10.0	3.16	17.33
20.0	4.47	17.32

Unloading Cycle - 31 kPa		
Time (t) [min]	Square root of time [min]	Deformation (s) [mm]
0.0	0.00	17.32
0.1	0.32	17.34
0.2	0.45	17.34
0.4	0.63	17.34
0.6	0.77	17.34
1.0	1.00	17.34
2.0	1.41	17.34
4.0	2.00	17.34
6.0	2.45	17.34
10.0	3.16	17.34

Unloading Cycle - 15.5 kPa		
Time (t) [min]	Square root of time [min]	Deformation (s) [mm]
0.0	0.00	17.35
0.1	0.32	17.38
0.2	0.45	17.38
0.4	0.63	17.38
0.6	0.77	17.38
1.0	1.00	17.38
2.0	1.41	17.38
4.0	2.00	17.38
6.0	2.45	17.38
10.0	3.16	17.38

Unloading Cycle - 8 kPa		
Time (t) [min]	Square root of time [min]	Deformation (s) [mm]
0.0	0.00	17.39
0.1	0.32	17.42
0.2	0.45	17.42
0.4	0.63	17.42
0.6	0.77	17.42
1.0	1.00	17.42
2.0	1.41	17.42
4.0	2.00	17.42
6.0	2.45	17.42

Unloading Cycle - 4 kPa		
Time (t) [min]	Square root of time [min]	Deformation (s) [mm]
0.0	0.00	17.43
0.1	0.32	17.45
0.2	0.45	17.45
0.4	0.63	17.46
0.6	0.77	17.46
1.0	1.00	17.46
2.0	1.41	17.46
4.0	2.00	17.46
6.0	2.45	17.46